JOURNAL OF COMPUTATIONAL PHYSICS 63, 416–433 (1986)

Transonic Flow Simulations Using an Upstream Centered Scheme of Godunov in Finite Elements

G. VIJAYASUNDARAM†

TIFR Centre, P. O. Box 1234, Bangalore 560012, India

Received June 22, 1983; revised January 15, 1985

A new first-order upwind scheme is presented and analysed. The scheme is simple to program and robust. The extension to a multi-dimensional FEM/FVM formulation is straightforward. The accuracy is demonstrated in two classical test cases. Results are obtained that do not contain unphysical oscillations even when FEM-type two-dimensional triangulations are used.

INTRODUCTION

The work reported here is part of a joint INRIA-AMDBA program for FEM-type simulations [2]. Early in this program it appeared that a robust first-order scheme for nonstructured (2-D) triangulations of (3-D) tetraedrization applying efficient boundary conditions procedures and having favourable matrix properties was needed.

First, a *new flux-splitting upwind scheme* has been designed. It has the following properties:

(1) It is first-order accurate (with monotone-like behaviour) but not very diffusive.

(2) Its assembling does not require a large computing time.

(3) Boundary conditions at infinity are self-handled.

(4) Its canonical linearization leads to a diagonally dominant matrix (in the scalar case), which can be trivially factored in lower–upper triangular matrices.

The last three properties are the result of our choice of an upwinding instead of using a Riemann solver.

The second feature of this paper is the fully multidimensional extension of the scheme to *nonstructured triangulations*. By nonstructured triangulations we mean FEM-type triangulations in which different nodes may have a different number of neighbors; this contrasts, for example, with a quadrangular FVM in which any given node always has four neighbors. The greater advantage of such triangulations

† Deceased.

0021-9991/86 $3.00

has been proven for aircraft design by the wide utilization of AMDBA's full potential transonic codes for such complex geometries as a complete trireactor jet [6].

In the discretizaton method, a choice has to be made on the location of nodes in the triangulation: P_1-type nodes, i.e., located at the vertices are chosen for the following reasons:

(1) The number of necessary nodes is less than in the case where the nodes are located at the centers of the triangles; this has a crucial importance for 3-D extensions.

(2) Nodes are located exactly on the boundary (in contrast with usual FVM approaches).

(3) The discretization is compatible with Galerkin FEM approximations. As a result, the discretization matrix can be utilized in a preconditioning process of the (more accurate) Galerkin approximations.

The resulting 2-D scheme is of FVM type for interior nodes and can be considered as derived from a variational FEM principle for wall boundary conditions. The stability is studied for simplified problems. The application to a well-known transonic test case is presented, which demonstrates precisely the accuracy of the approximation. In the past, first-order monotone-type schemes have been constructed based on two main approaches:

(i) Upwinding has been prompted by Courant–Isaacson–Rees [5], and extensively used by Moretti [10] for nonconservative scheme and Steger–Warming [16], Lerat [8], and Van Leer [19] for conservative schemes.

(ii) Riemann solvers, developed mainly by Godunov [7] have been used by Roe [14] and Osher [12].

Several of the above authors have noted that Riemann Solvers could very well be approximated roughly without unduly deteriorating the accuracy. Although the scheme presented here could be interpreted as one that uses a (very) approximate Riemann Solver, it should be considered as a flux-splitting scheme, analogous to the Steger and Warming [16] scheme.

In Section 1, a one-dimensional upstream-centered finite-difference scheme is derived from the characteristic form of the equations. Section 2 deals with the extension of the scheme to finite elements. A linear stability analysis is carried out in Section 3. The numerical experiments follow in Section 4.

1. One-Dimensional Upstream-Centered Finite-Difference Scheme

The Euler equations of gas dynamics in conservation form are written as

$$W_t + F(W)_x = 0, \tag{1}$$

where

$$W = \begin{pmatrix} \rho \\ \rho u \\ e \end{pmatrix}, \qquad F(W) = \begin{pmatrix} \rho u \\ \rho u^2 + p \\ (e+p)u \end{pmatrix} \tag{2}$$

$$p = (\gamma - 1)(e - \tfrac{1}{2}\rho u^2), \qquad \gamma = 1.4; \tag{3}$$

ρ is the density of the gas, u is the velocity, e is the total energy per unit volume, p is the pressure, and γ is the ratio of specific heats.

The flux vector F is a homogeneous function of degree one,

$$F(\alpha W) = \alpha F(W), \qquad \forall \alpha \in \mathbb{R},\ W \in \mathbb{R}^3. \tag{4}$$

As a consequence of (4) we have

$$F(W) = F'(W)\, W, \qquad \forall W \in \mathbb{R}^3. \tag{5}$$

The Jacobian matrix $A = F'(W)$ is diagonalisable and can be put in the form

$$A(W) = T(W)\, \Lambda(W)\, T^{-1}(W). \tag{6}$$

Equation (1) has the nonconservative form

$$W_t + A(W)\, W_x = 0 \tag{7}$$

and the characteristic form

$$T^{-1}(W)\, W_t + \Lambda(W)\, T^{-1}(W)\, W_x = 0. \tag{8}$$

The component equations of (8) are

$$\sum_{k=1}^{3} T_{jk}^{-1}(W) \left(\frac{\partial}{\partial t} + \lambda_j(W) \frac{\partial}{\partial x} \right) W_k = 0, \qquad 1 \leqslant j \leqslant 3, \tag{9}$$

where

$$T^{-1} = (T_{jk}^{-1}), \qquad W = (W_k), \qquad \Lambda(W) = \operatorname{diag}\{\lambda_k(W)\}.$$

In (9), the components of W are differentiated along the same characteristic direction λ_j. Equation (9) suggests to us that we use a centered approximation for $T_{jk}^{-1}(W)$, $\lambda_j(W)$ and a one-sided differencing for the space derivative based on the sign of λ_j.

A semi-discrete explicit approximation of (1) to first-order accuracy is

$$\frac{W^{n+1} - W^n}{\Delta t} + F(W^n)_x = 0, \tag{10}$$

where

$$W^n = W(x, t^n), \qquad \Delta t = t^{n+1} - t^n.$$

Let x_i, $i \in Z$ be the grid points with mesh width Δx. The approximate test functions are taken to be piecewise functions constant in the interval $[x_{i-1/2}, x_{i+1/2}]$ where $x_{i+1/2} - x_i + (\Delta x/2)$. The Rayleigh–Ritz–Galerkin approximation consists to find W_h^{n+1} in the approximate test function space V_h such that

$$\int_{\mathbb{R}} \frac{W_h^{n+1} - W_h^n}{\Delta t} v_h \, dx + \int_{\mathbb{R}} F(W_h^n)_x \, v_h \, dx = 0, \qquad \forall v_h \in V_h. \tag{11}$$

Since the characteristic functions χ_i of the interval $[x_{i-1/2}, x_{i+1/2}]$ form a base for V_h, Eq. (11) holds iff it is true for each χ_i. Taking $v_h = \chi_i$ in (11) and using integration by parts for the second integral we arrive at the finite difference scheme

$$\frac{W_i^{n+1} - W_i^n}{\Delta t} \Delta x + (\phi_F)_{i+1/2}^n - (\phi_F)_{i-1/2}^n = 0, \tag{12}$$

where

$$W_i^n = W_h^n|_{[x_{i-1/2}, x_{i+1/2}]}, \qquad (\phi_F)_{i+1/2}^n = F(W_{i+1/2}^n).$$

As the function W_h^n is discontinuous at the points $x_{i+1/2}^n$, $(\phi_F)_{i+1/2}^n$ cannot be defined in a unique way. It has to be defined as a function of W_i^n and W_{i+1}^n in a consistent manner:

$$((\Phi_F)_{i+1/2}^n = \Phi_F(W_i^n, W_{i+1}^n), \qquad \Phi_F(W, W) = F(W).$$

By defining $\Phi_F(W, \bar{W}) = (F(W) + F(\bar{W}))/2$, Eq. (12) becomes a centered difference scheme which is not stable.

The upstream-centered conservative scheme suggested by (9) has the numerical flux

$$(\Phi_F)_{i+1/2}^n = (F'(W)W)_{i+1/2}^n = (T\Lambda)_{i+1/2}^{n,c} (T^{-1}W)_{i+1/2}^{n,cu}, \tag{13}$$

where

$$(T\Lambda)_{i+1/2}^{n,c} = (T\Lambda)(W_{i+1/2}^n), \quad W_{i+1/2}^n = \frac{W_i^n + W_{i+1}^n}{2},$$

$$(T^{-1}W)_{i+1/2}^{n,cu} = \left(\sum_{k=1}^{m} (T_{jk}^{-1})_{i+1/2}^n (W_k)_{(\alpha_j)_{i+1/2}^n}^n \right)_{j=1}^{m},$$

$$(\alpha_j)_{i+1/2}^n = \begin{cases} i & \text{if } \lambda_j(W_{i+1/2}^n) > 0 \\ i+1 & \text{otherwise,} \end{cases}$$

$$(T_{jk}^{-1})_{i+1/2}^n = T_{jk}^{-1}(W_{i+1/2}^n).$$

With the notation

$$A = F' = T\Lambda T^{-1}, \qquad A^{\pm} = T\Lambda^{\pm} T^{-1},$$
$$\Lambda^{\pm} = \operatorname{diag}\{\lambda_k^{\pm}\}, \qquad (A^{\pm})^n_{i+1/2} = A^{\pm}(W^n_{i+1/2}),$$
$$\lambda_k^{+} = \max(\lambda_k, 0), \qquad \lambda_k^{-} = \min(\lambda_k, 0)$$

the numerical flux (13) can be written in the form

$$(\Phi_F)^n_{i+1/2} = (A^{+})^n_{i+1/2} W^n_i + (A^{-})^n_{i+1/2} W^n_{i+1}. \tag{14}$$

This splitting is different from that of Steger and Warming [16] (see also Lerat [8] for a similar scheme),

$$(\Phi_{SW})^n_{i+(1/2)} = (A^{+})^n_i W^n_i + (A^{-})^n_{i+1} W^n_{i+1}. \tag{15}$$

We shall see in Section 4 that the results obtained from these schemes show large variations.

At the contrary, scheme (14) is similar to Van Leer's Q-scheme (see [19]; Van Leer calls it *Godunov's scheme*),

$$(\Phi_{VL})^n_{i+(1/2)} = \frac{F(W^n_i) + F(W^n_{i+1})}{2} = \frac{1}{2}[(A^{+})^n_{i+(1/2)} - (A^{-})^n_{i+(1/2)}](W^n_{i+1} - W^n_i). \tag{16}$$

2. Two-Dimensional Scheme

The inviscid gas dynamic equations in two dimensions and in conservation-law form are

$$W_t + F(W)_x + G(W)_y = 0,$$

$$W = \begin{pmatrix} \rho \\ \rho u \\ \rho v \\ e \end{pmatrix}, \qquad F(W) = \begin{pmatrix} \rho u \\ \rho u^2 + p \\ \rho uv \\ (e+p)u \end{pmatrix}, \qquad G(W) = \begin{pmatrix} \rho v \\ \rho uv \\ \rho v^2 + p \\ (e+p)v \end{pmatrix}, \tag{17}$$

$$p = (\gamma - 1)\left(e - \frac{1}{2}\rho(u^2 + v^2)\right), \qquad \gamma = 1.4. \tag{18}$$

An explicit, first-order accurate time-discretization of (17) is

$$\frac{W^{n+1} - W^n}{\Delta t} + F(W^n)_x + G(W^n)_y = 0. \tag{19}$$

Let τ_h be a triangulation of the computational domain Ω consisting of triangular elements. A restructuring of the triangulation is done by constructing disjoint cells,

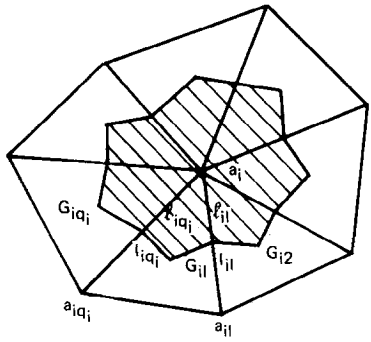

FIG. 1. Integration cell (a_i).

each cell containing exactly one node of the triangulation. This is accomplished by joining the centroids of the triangles having a node as a common vertex and the midpoints of the sides passing through that node (Figs. 1 and 2: the following notations are used: q_i is the number of triangles around the node a_i, K_{ij}, $1 \leqslant j \leqslant q_i$, triangles with a_i as a common vertex, G_{ij}, centroid of the triangle a_{ij}, a_{ij}, $1 \leqslant j \leqslant q_i$, neighbouring nodes around a_i, I_{ij}, midpoint of the side $a_i a_{ij}$, Cell(a_i), region bounded by the segments $G_{i1}I_{i1}$, $I_{i1}G_{i2}$,..., $G_{iq_i}I_{iq_i}$, I_{iq_i}, G_{i1}, and Ar(a_i), area of the cell (a_i)).

In Fig. 1 Cell(a_i) is shaded.

The approximation test function space V_h consists of piecewise constant functions, constant in each cell. The approximation problem is to find $W_h^{n+1} \in V_h$ such that

$$\int_\Omega \frac{W_h^{n+1} - W_h^n}{\Delta t} v_h \, dx \, dy + \int_\Omega \{F(W_h^n)_x + G(W_h^n)_y\} \, v_h \, dx \, dy = 0, \qquad \forall v_h \in V_h. \quad (20)$$

As characteristic functions of the cells form a base for V_h. (20) holds iff the

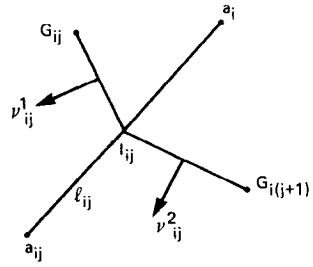

FIG. 2. Segment through a_i.

equation holds good for each characteristic function. Using Green's formula, we have

$$\frac{W_i^{n+1} - W_i^n}{\Delta t} \operatorname{Ar}(a_i) + \sum_{j=1}^{q_i} \left(\int_{G_{ij}I_{ij}} + \int_{I_{ij}G_{i(j+1)}} \right) \{F(W_h^n)\, v_x + G(W_h^n)\, v_y\}\, d\sigma = 0, \tag{21}$$

where

$$W_i^n = W_h^n|_{\text{cell}(a_i)}, \qquad W_{ij}^n = W_h^n|_{\text{cell}(a_{ij})}.$$

Equation (21) reduces to

$$\frac{W_i^{n+1} - W_i^n}{\Delta t} \operatorname{Ar}(a_i) + \sum_{j=1}^{q_i} \Phi_{H_{ij}}^n = 0, \tag{22}$$

$$H_{ij} = \eta_{xij} F + \eta_{yij} G, \qquad \eta_{ij} = (\eta_{xij}, \eta_{yij}),$$

$$\eta_{ij} = v_{ij}^1 |G_{ij} I_{ij}| + v_{ij}^2 |I_{ij} G_{i(j+1)}|,$$

v_{ij}^1, outward drawn unit normal to the segment $G_{ij}I_{ij}$ with respect to the cell(a_i), v_{ij}^2, outward unit normal to the segment $I_{ij}G_{i(j+1)}$ with respect to the cell(a_i), H_{ij}^n, one-dimensional first-order accurate numerical flux

$$\Phi_{H_{ij}}^n = \Phi_{H_{ij}}(W_i^n, W_{ij}^n). \tag{23}$$

3. Linear Stability Analysis

In one dimension, for the linear case, Godunov scheme takes the form

$$\frac{(T^{-1}W)_i^{n+1} - (T^{-1}W)_i^n}{\Delta t} \Delta x + \Lambda^+ (T^{-1}W)_i^n + \Lambda^- (T^{-1}W)_{i+1}^n$$

$$- \Lambda^+ (T^{-1}W)_{i-1}^n - \Lambda^- (^{-1}W)_i^n = 0. \tag{24}$$

Equation (24) corresponds to three scalar equations

$$\frac{(T^{-1}W)_{ki}^{n+1} - (T^{-1}W)_{ki}^n}{\Delta t} \Delta x + \lambda_k^+ (T^{-1}W)_{ki}^n + \lambda_k^- (T^{-1}W)_{k(i+1)}^n$$

$$- \lambda_k^+ (T^{-1}W)_{k(i-1)}^n - \lambda_k^- (T^{-1}W)_{kj}^n = 0, \qquad 1 \leqslant k \leqslant 3, \tag{25}$$

where $(T^{-1}W)_{ki}^n$ is the kth component of the vector $(T^{-1}W)_i^n$.

The scalar schemes (25) are stable and monotone if

$$\max_{1 \leqslant k \leqslant 3} |\lambda_k| \frac{\Delta t}{\Delta x} \leqslant 1. \tag{26}$$

For the two-dimensional linear case for uniform mesh Godunov Scheme (22) becomes

$$\frac{W_i^{n+1} - W_i^n}{\Delta t} \mathrm{Ar}(a.) + \sum_{j=1}^{6} H_{.j}^{+} W_i^n + H_{.j}^{-} W_{ij}^n = 0 \tag{27}$$

the quantities $\mathrm{Ar}(a_i)$, $H_{ij}^{\pm}$ being independent of i, the subscript i is replaced by dot.

Equation (27) can be written as

$$W_i^{n+1} = \left(I - \frac{\Delta t}{\mathrm{Ar}(a.)} \sum_{j=1}^{6} H_{.j}^{+} \right) W_i^n + \sum_{j=1}^{6} \frac{\Delta t}{\mathrm{Ar}(a.)} H_{.j}^{-} W_{ij}^n.$$

Only in the special case $H_{.j} = T \Lambda_{.j} T^{-1}$ stability and monotonic follows trivially under the CFL condition

$$\max_{\substack{1 \leqslant j \leqslant 6 \\ 1 \leqslant k \leqslant 4 \\ i,n}} |\lambda_{kij}^n| \frac{\Delta t}{\mathrm{Ar}(a_i)} \leqslant 1. \tag{28}$$

An analogous condition has been obtained by Osher [11] in a constant by triangle FEM context.

4. Numerical Experiments

The above scheme is applied to the Euler equations. Similarity matrices can be found in [3].

Scheme (22) is applied first to shock tube problem proposed by Sod [15]. A thin diaphragm separates two gases at different states which both are at rest at $t = 0$. When the diaphragm is burst an expansion wave travels into the region of low pressure and a shock wave followed by contact surface moves into the region of high pressure. The exact solution of this problem is known and can be found in Whitham [21].

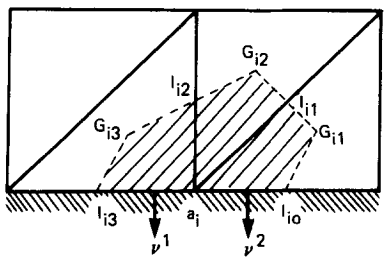

FIG. 3. Boundary cell around the node a_i. Segments $I_{i3}a_i$ and a_iI_{i0} are solid wall segments.

The initial conditions are

$$u=0, \quad v=0, \quad p=1.0, \quad \rho=1.0 \qquad \text{if } x<0.5$$
$$u=0, \quad v=0, \quad p=0.1, \quad \rho=0.125 \qquad \text{if } x>0.5.$$

A 101×3 mesh is used. Distributions of density, pressures, horizontal velocity and internal energy at time $t=0.1619$ are presented in Fig. 4, with a CFL number of 0.9.

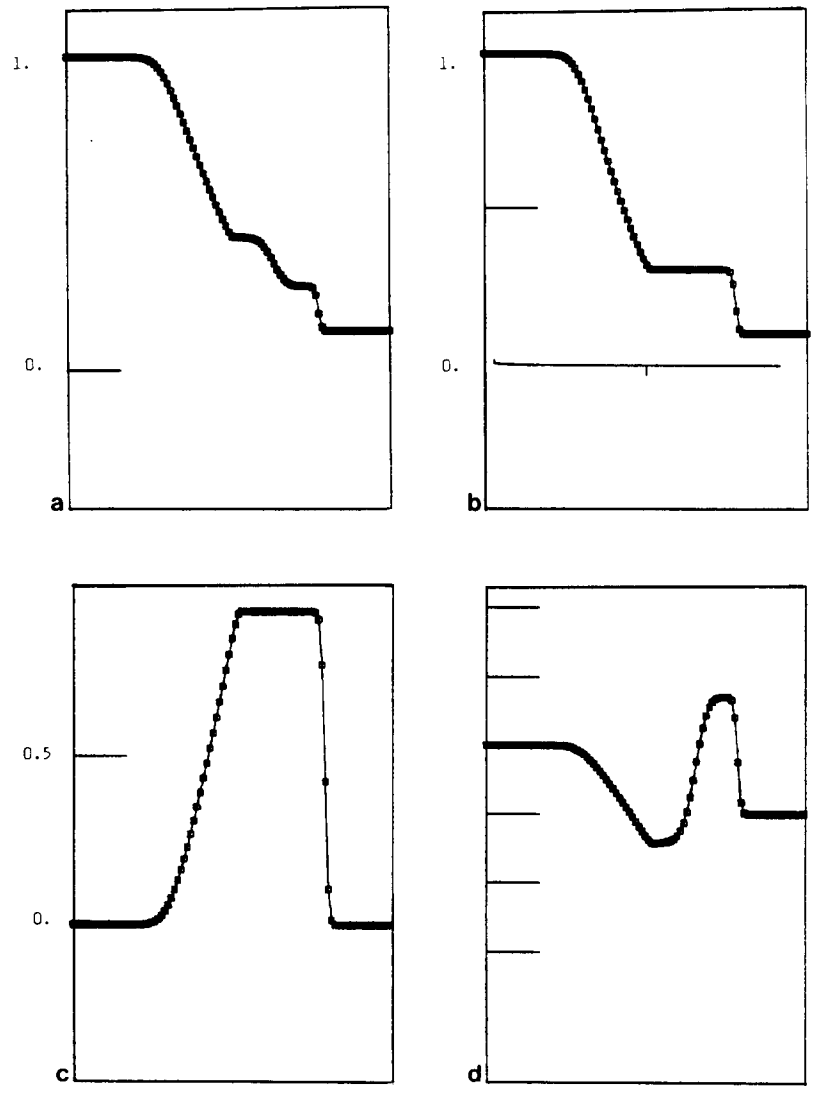

FIG. 4. The shock tube problem: 2-D scheme (density, pressure, velocity, temperature at time 0.165).

The results obtained are comparable with the 1-D results of G. Sod [15] using a two-step version of Godunov's scheme. They are nearly identical to the (2-D) results obtained with scheme (16), presented in Fig. 5 (The shock is slightly sharper in Fig. 4), while much more dissipation is observed with the 2-D version of scheme (15) (Fig. 6).

The scheme is also applied to the problem B proposed at the GAMM Workshop [13]. A channel of length 5.0 and height 2.073 units contains a circular arc profile as a part of the bottom solid wall at a distance of 2.0 units from the inlet.

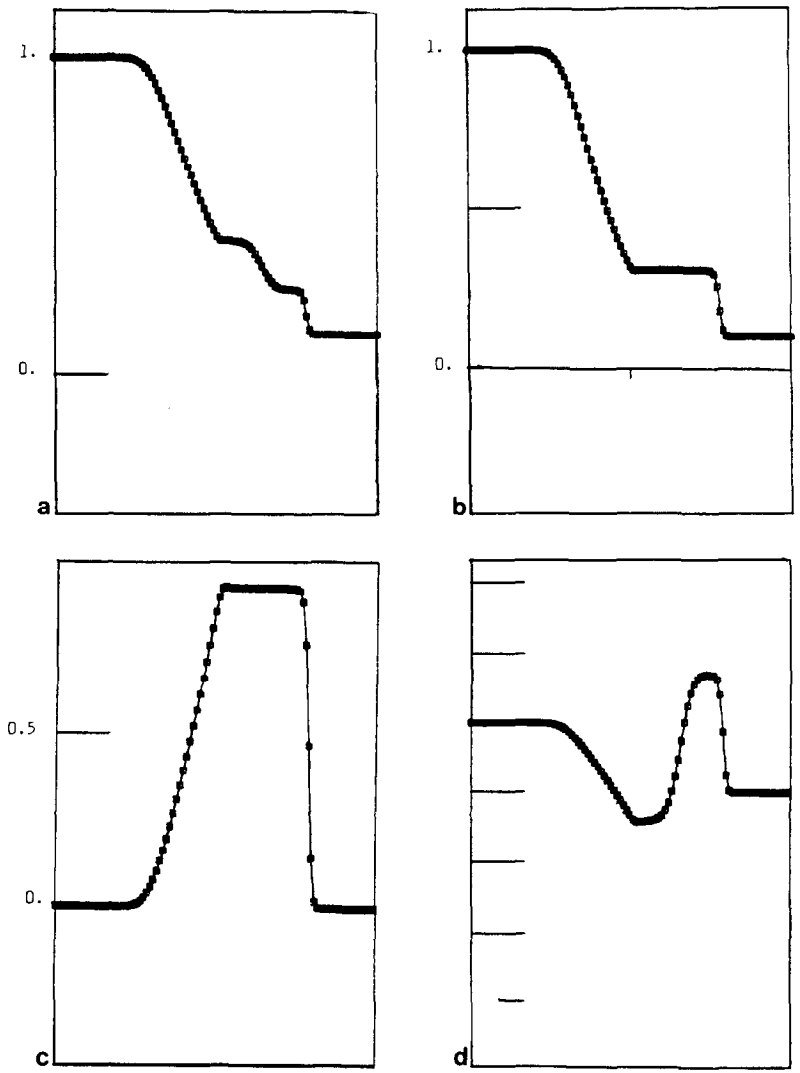

FIG. 5. The shock tube problem: 2-D version of Van Leer's (first-order) scheme (16).

The thickness of the arc is equal to 4.2% of the chord. A 72×21 finite element triangulation which is comparable with the one proposed by GAMM is used.

The initial condition is an incompressible perturbation of a uniform flow. Far field boundary conditions are specified as

$$M_\infty = 0.85, \quad \rho_\infty = 1.0, \quad u_\infty = 1.0, \quad v_\infty = 0.0.$$

At solid walls tangential velocity condition is imposed as the boundary condition.

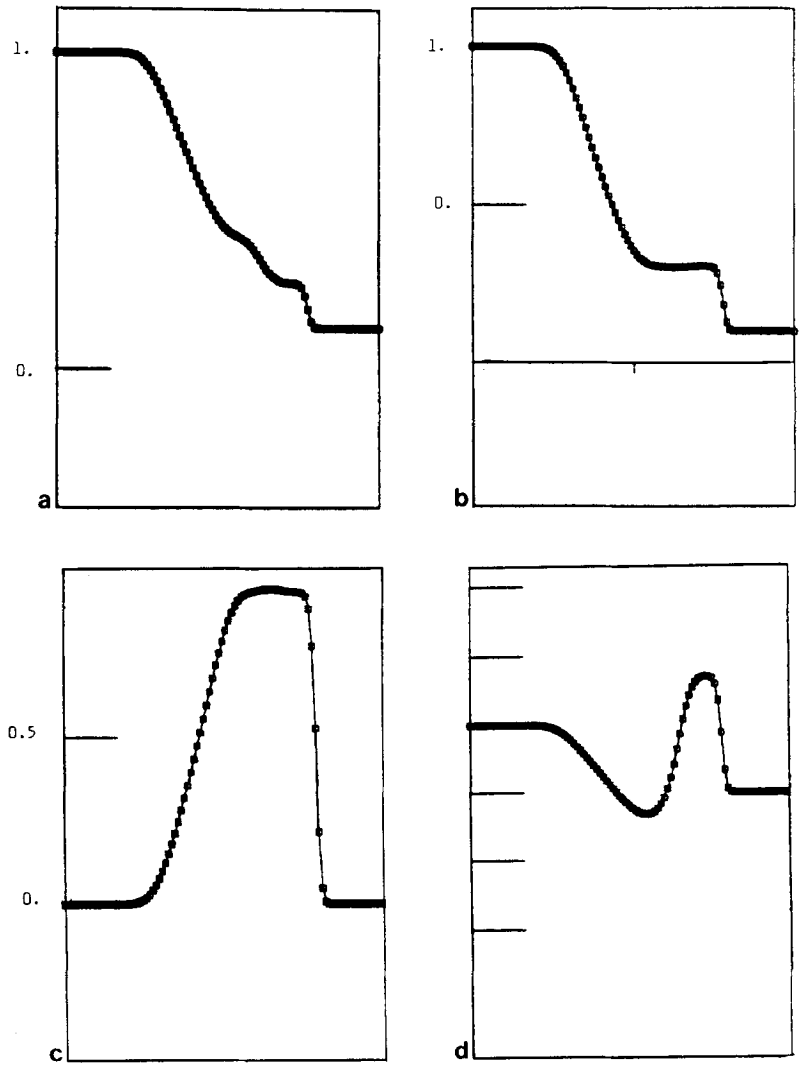

FIG. 6. The shock tube problem: 2-D version of Steger and Warming's and Warming's (first-order) scheme (15).

Solid wall boundary integral is calculated as (see Fig. 3),

$$\int_{I_{i3}a_iI_{i0}} (v_x F + v_y G)\, d\sigma = \int \left\{ (v_x u + v_y v) W + p \begin{bmatrix} 0 \\ v_x \\ v_y \\ 0 \end{bmatrix} \right\} d\sigma$$

$$= p(a_i) \begin{bmatrix} 0 \\ v^1 |I_{i3} a_i| + v_x^2 |a_i I_{i0}| \\ v_y^1 |I_{i3} a_i| + v_y^2 |a_i I_{i0}| \\ 0 \end{bmatrix},$$

At the inlet and outlet far field boundary, conditions of uniform flow are forced after each time step; upstream values for inflow boundary (resp. downstream values for outflow boundary) are automatically selected by the upwind scheme [20].

Norm in l^2 of $\Delta\rho/\Delta t$ is taken as a measure of residue. cpu time taken per iteration is 8.47 sec in CII-HB DPS-68. It took 1000 iterations to arrive at a residue of the order 10^{-4}. After 4500 iterations residue was steadily decreasing. The scheme converged to the steady state in 8900 iterations with a residue of the order 10^{-6}.

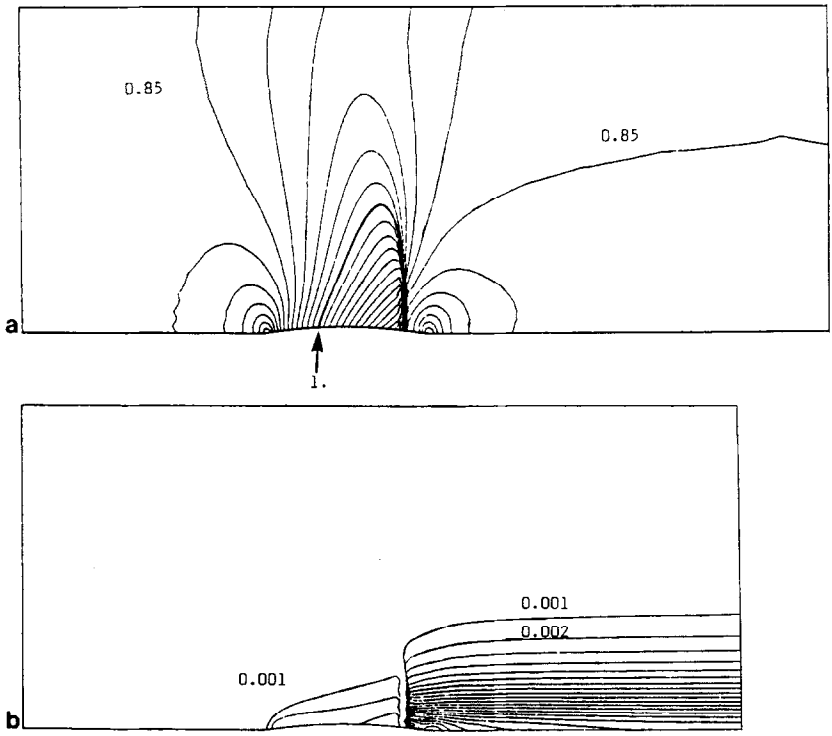

FIG. 7. GAMM test problem with presented scheme: iso-Mach and isentropic lines.

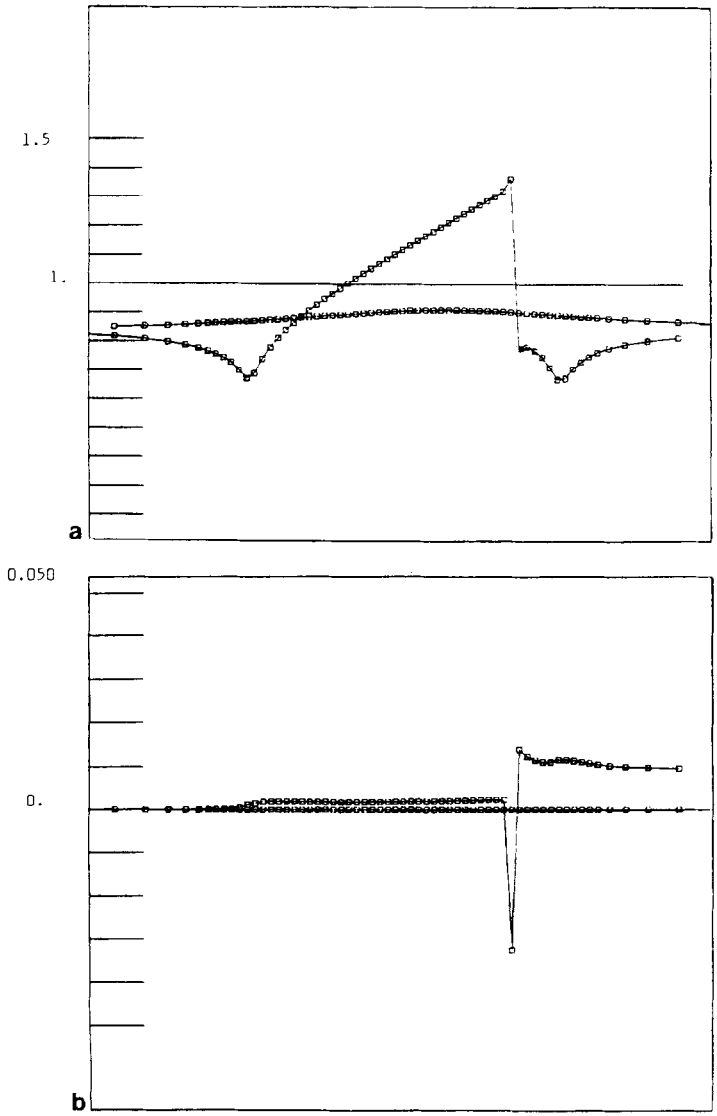

FIG. 8. GAMM test problem with presented scheme: Mach and entropy deviation distributions at the bottom.

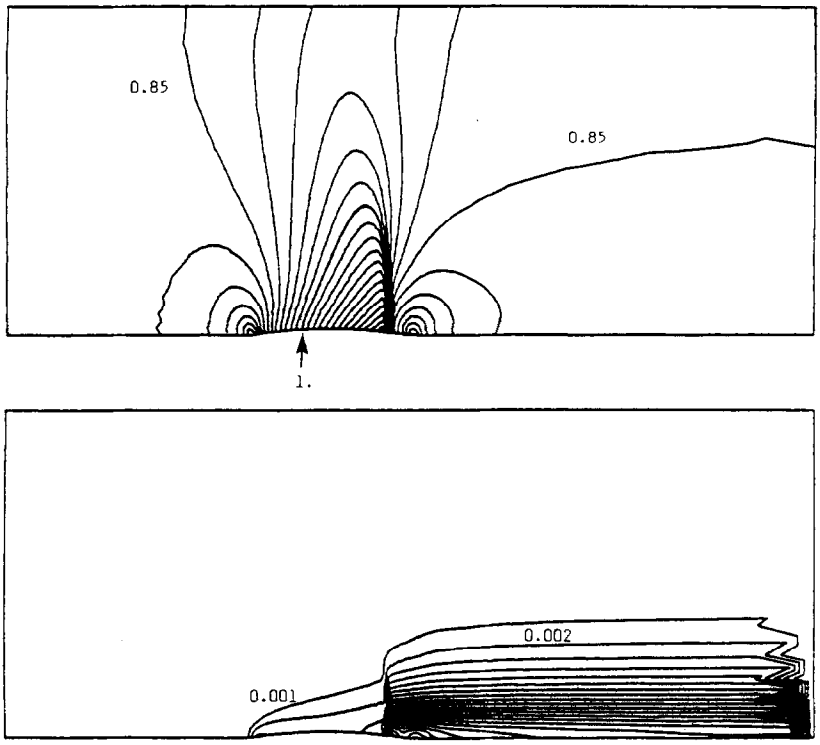

FIG. 9. GAMM test problem with the 2-D version of Van Leer's scheme (16): iso-Mach and isentropic lines.

Iso-Mach lines and isentropic lines are presented in Fig. 7, and the distributions of Mach and entropy deviation on the bottom solid wall are shown in Fig. 8. The shock is sharp with no point on it; there is a slight overshoot; entropy deviation ahead the shock is about 0.3×10^{-2}.

The results obtained are comparable with those of Borrel and Morice [4] and Lerat and Sides [9].

While the Q-scheme (16) did not show any striking difference for the shock tube test, it exhibits a different behaviour in the presence of a stationary shock as is observed in Figs. 9 and 10. Monotony is better preserved by scheme (16) but it is not always true that we prefer shocks with three transition zones. Furthermore, scheme (16) is more computer time consuming.

Comparisons with Steger and Warming's scheme (15) shows again, even with this refined mesh, a larger amount of viscosity for scheme (15), see Figs. 11 and 12.

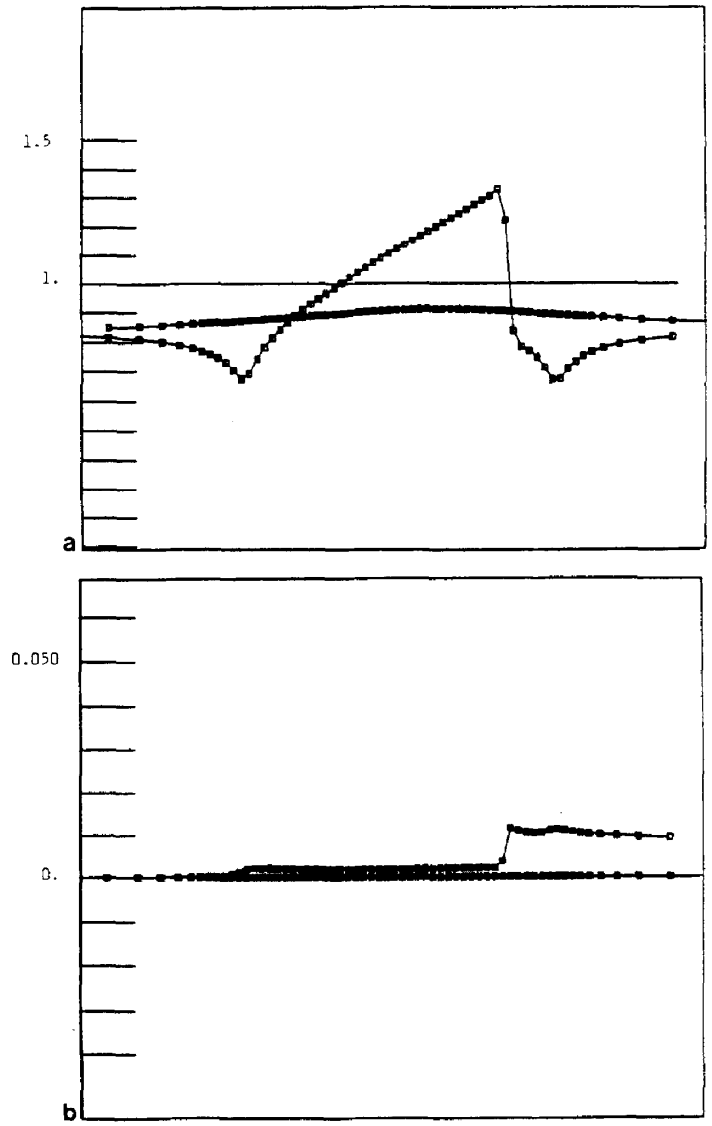

FIG. 10. GAMM test problem with the 2-D version of Van Leer's scheme (16). Mach and entropy distributions at the bottom.

5. Concluding Remarks

The numerical scheme presented in this paper is

(i) efficient, in terms of computing time,

(ii) simple to program,

(iii) robust,

(iv) at least as accurate as many other usual first-order schemes (it introduces relatively small amounts of artificial dissipation, and stationary shocks are quite sharp).

The scheme can adequately be applied to the simulation of strongly shocked flows. Its good matrix properties allow it to be used in a preconditioning procedure of a second-order solver. Since the time this paper was submitted, this numerical scheme has also been applied to the calculation of the mixed internal–external flow past an inlet [2] and the simulation of some 3-D flows. This spatial approximation

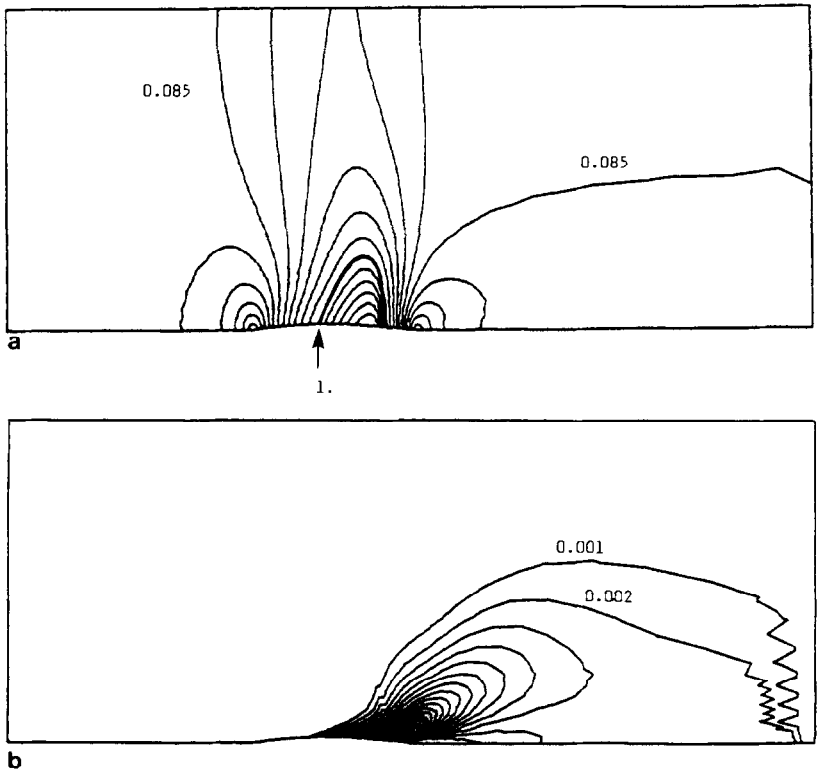

FIG. 11. GAMM test problem with the 2-D version of steger and Warming's scheme (15): iso-Mach and isentropic lines.

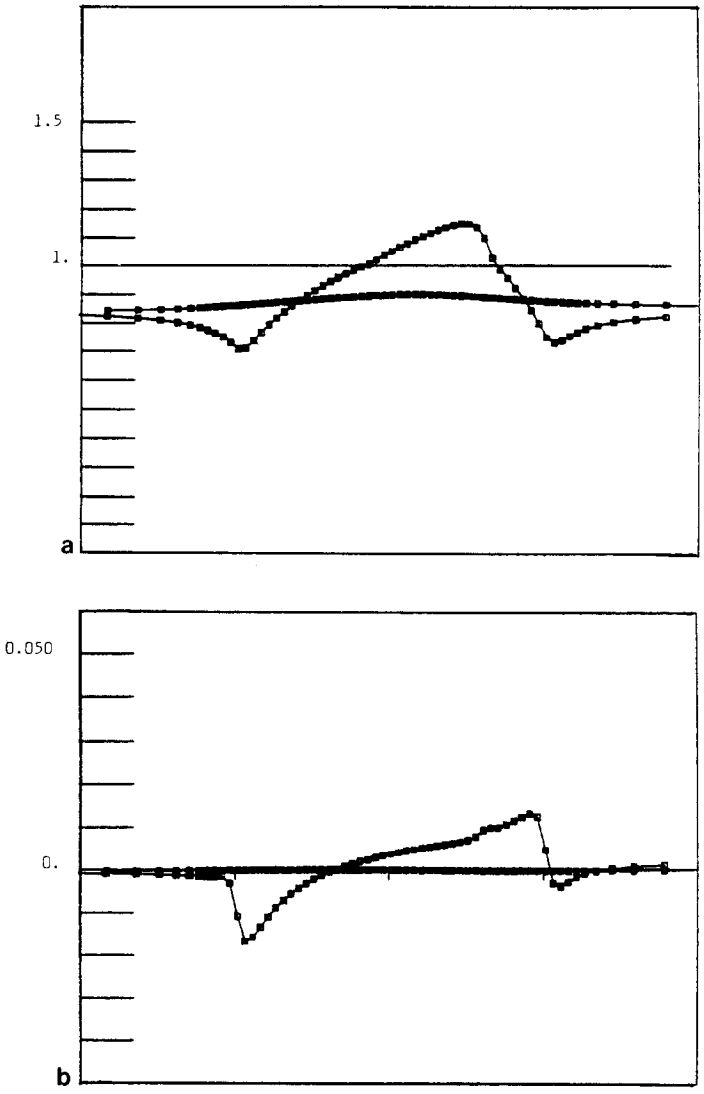

FIG. 12. GAMM test problem with the 2-D version of Steger and Warming's scheme (15): Mach and entropy distributions at the bottom.

has been used also in conjunction with a new explicit time-stepping scheme [17], as a preconditioning procedure of a second-order implicit scheme [18].

ACKNOWLEDGMENTS

The author wishes to thank Professor Glowinski, Professor Pironneau, Dr. Dervieux, and Dr. Angrand for the fruitful discussions he had with them. The above work was carried out during the author's stay at INRIA, France. The author acknowledges with thanks INRIA and TIFR, India for financial support.

REFERENCES

1. F. ANGRAND AND A. DERVIEUX, *Int. J. Numer. Methods Fluids* **4** (1984), 749.
2. F. ANGRAND, V. BOULARD, A. DERVIEUX, J. PERIAUX, AND G. VIJAYASUNDARAM, Transonic Euler Simulations by means of Finite Element explicit Schemes, AIAA paper p. 83, 1983.
3. R. M. BEAM AND R. F. WARMING, *J. Comput. Phys.* **22** (1976), 87.
4. M. BORREL AND PH. MORICE, *in* "Proceedings, Fourth GAMM Conference on Numerical Methods in Fluid Mechanics" (H. Viviand, Ed.), Vieweg Sohn, Braunschweig–Wiesbaden, 1982.
5. R. COURANT, E. ISAACSON, AND M. REES, *Commun. Pure Appl. Math.* **5** (1952), 243.
6. R. GLOWINSKI AND J. PERIAUX, *in* "Von Karman Institute for Fluid Dynamics, Lecture Series," 1983-04, Computational Fluid Dynamics, March 7–11, 1983.
7. S. K. GODUNOV, *Mat. Sb.* **47** 271, (1959), Cornell Aeronautical Lab. Transl.
8. A. LERAT, *J. Mec. Theor. Appl.* **2** No. 2, (1983), 185.
9. A. LERAT AND J. SIDES, *in* "Notes on Numerical Fluid Mechanics," Vol. 3, p. 142. Vieweg & Sohn, Braunschweig/Wiesbaden, 1981.
10. F. MORETTI, *Comput. Fluids* **7** (1979), 191.
11. S. OSHER, *C. R. Acad. Sci. Paris Ser. A* **290** (1980), 819.
12. S. OSHER AND F. SOLOMON, *J. Math. Comput.* (1982).
13. A. RIZZI AND H. VIVIAND, *in* "Notes on Numerical Fluid Mechanics," Vol. 3, "Numerical Methods for the Computation of Inviscid Transonic Flows with Shock Waves," Vieweg & Sohn, Braunschweig/Wiesbaden, 1981.
14. P. L. ROE, *in* "Proceedings, 7th Int. Conf. on Numer. Methods in Fluid Dynamics, Stanford, 1980," Springer-Verlag, Berlin/New York, 1981.
15. G. A. SOD, *J. Comput. Phys.* **27**, (1978), 1.
16. J. STEGER AND R. F. WARMING, *J. Comput. Phys.* **40** (1981), 263.
17. B. STOUFFLET, thesis, University of Paris VI, 1984.
18. B. STOUFFLET, Contribution to the Workshop on Numerical Methods for the Euler Equations for Compressible Inviscid Flows" (R. Glowinski, Ed.).
19. B. VAN LEER III, *J. Comput. Phys.* **23** (1977), 263.
20. G. VIJAYASUNDARAM, "Résolution numérique des équations d'Euler pour des écoulements transoniques avec un schéma to Godunov en élément finis," thésis, Université de Pierre et Marie Curie, Paris VI, 1983.
21. G. B. WHITHAM, "Linear and Nonlinear Waves," Wiley–Interscience, New York, 1974.